Virus Research 352 (2025) 199518

Contents lists available at ScienceDirect

Virus Research

journal homepage: www.elsevier.com/locate/virusres

Infectivity in full-term placenta of Zika viruses with different lipid profiles

Eva Mazzetto [a,b,*], Alessio Bortolami [b], Davide Bovo [c], Matteo Stocchero [a,c], Elisa Mazzacan [b], Alessandra Napolitan [b], Valentina Panzarin [d], Maria Rosa Tran [e], Gianpiero Zamperin [d], Adelaide Milani [d], Andrea Fortin [d], Michela Bigolaro [f], Paola Pirillo [a,c], Matteo Pagliari [a,b], Claudia Zanardello [f], Giuseppe Giordano [a,c], Maria Teresa Gervasi [e], Eugenio Baraldi [a,c], Calogero Terregino [b], Carlo Giaquinto [a], Francesco Bonfante [b]

[a] Department of Women's and Children's Health, Padua University, Padova (PD), Italy
[b] Department of Virology, Istituto Zooprofilattico Sperimentale delle Venezie, Legnaro (PD), Italy
[c] Laboratory of Mass Spectrometry and Metabolomics, Department of Women's and Children's Health, Padua University, Padova (PD), Italy
[d] Department of Research and Innovation, Istituto Zooprofilattico Sperimentale delle Venezie, Legnaro (PD), Italy
[e] Gynaecology and Obstetrics Unit, Department of Women's and Children's Health, Padua University, Padova (PD), Italy
[f] Department of Diagnostic Services, Histopathology, Parasitology, Istituto Zooprofilattico Sperimentale delle Venezie, Legnaro (PD), Italy

ARTICLE INFO

Keywords:
ZIKV
Lipids
Placenta
Explants
Lipidomic

ABSTRACT

Among flaviviruses, Zika virus (ZIKV) is the only arbovirus officially recognized as a teratogenic agent, as a consequence of its ability to infect and cross the placental barrier causing congenital malformation in the fetus. While many studies have focused on understanding ZIKV pathogenesis during pregnancy, the viral mechanisms affecting fetal development remain largely unclear. In this study, we investigated ZIKV virulence in placental trophoblasts, using viruses with distinct lipid profiles. Firstly, we propagated a ZIKV strain belonging to the Asian lineage in either mammalian or mosquito cells, obtaining two viral stocks, which were purified and analyzed to determine their genetic and lipid composition. Successively, we assessed the infectivity of the two stocks in placental cells using both immortalized cell lines and explants. We found that the two viral stocks displayed identical consensus sequences with homogeneous quasispecies composition. However, the lipid composition of their envelope significantly varied depending on the cell of origin, with the mammalian-derived viral stock characterized by a higher content of phosphatidylcholines compared to the virions originating from mosquito cells. Notably, ZIKV stock derived from mammalian cells showed a higher infectivity in immortalized villous trophoblasts and full-term placental explants of human origin. This increased infectivity was linked to enhanced fusion efficiency during the viral uncoating phase in trophoblast cells, as demonstrated using a lipophilic probe. Collectively, our data suggest a potential role of viral lipids as determinants of ZIKV infectivity in full-term placenta, underscoring the importance of lipidomic research in virology.

1. Introduction

ZIKA virus (ZIKV), an arbovirus of the Flaviviridae family, has been recognized as the first vector-born agent among TORCH (Toxoplasma gondii, other, Rubella virus, Cytomegalovirus and Herpes simplex virus) (CB Coyne and Lazear, 2016). In pregnant women, ZIKV infection can severely affect fetal development, ranging from miscarriage to the so-called congenital ZIKV syndrome (CZS), characterized by a combination of microcephaly, arthrogryposis, fetal growth reduction and other neurological and developmental disorders (Ades et al., 2021). These clinical outcomes depend on the virus ability to cross the placental barrier impairing the regular neuronal development of the fetus. However, the pathogenic mechanisms behind ZIKV vertical transmission remain elusive (Villalobos-Sánchez et al., 2022). Numerous *in-vitro* and *in-vivo* studies have demonstrated that, in the first trimester, several placental cells including the extravillous trophoblasts (EVT), villous cytotrophoblasts (CTB), fibroblast cells and Hofbauer cells are highly susceptible to ZIKV infection (Tabata et al., 2016). In contrast, in the mid and late trimesters of gestation, syncytiotrophoblasts (STBs) differentiated from the underlying proliferative CTB cells (Arora et al., 2016)

* Corresponding author.
E-mail address: emazzetto@izsvenezie.it (E. Mazzetto).

https://doi.org/10.1016/j.virusres.2024.199518
Received 16 October 2024; Received in revised form 9 December 2024; Accepted 19 December 2024
Available online 6 January 2025

provide additional defenses, actively secreting type III interferon (A Bayer et al., 2017). Despite these protective mechanisms, longitudinal studies indicate impairments in fetal neuronal development and sensory dysfunctions in children born from mothers infected during the second and third trimesters, implying that the virus can elude or compromise STBs barrier at this stage as well (Brasil et al., 2020, Einspieler et al., 2019, Noronha et al., 2018). The gap in knowledge regarding the determinants of ZIKV virulence in the fetus and the mechanisms employed by the virus to cross the placenta hampers the development of an effective prophylactic and post-exposure treatment for pregnant women.

In the last decade, lipidomics has yielded new insights on the highly complex interplay between the Flaviviridae family and lipids, demonstrating that both viral and host cell membrane lipids play key roles in the replicative cycle (Leier et al., 2020, Melo et al., 2016, Queiroz et al., 2019). At the first stage, plasma membrane lipid rafts can provide a suitable environment by concentrating the viral receptors and acting as cellular signal transduction platforms to promote the viral attachment (Martín-Acebes et al., 2016). Moreover, lipids of Flavivirus envelope are recognized by multiple cellular receptors that belong to the families of the transmembrane phosphatidylserines, which contribute to bind and internalize viral particles (Agrelli et al., 2019). The lipid composition of both viral and host cell membranes can also influence the efficiency of fusion between Flaviviridae and the endosome leading to viral uncoating and the initiation of viral replication (Zaitseva et al., 2010, Gollins and Porterfield, 1986, Carro and Damonte, 2013). Furthermore, during viral replication, flaviviruses severely affect host-cell lipid machinery to create a favorable environment for viral multiplication (Leier et al., 2020, Leier et al., 2018, Perera et al., 2012).

Despite a growing body of evidence has pointed out how lipids are fundamental for the fitness of flaviviruses, the scientific literature on viral lipids as drivers of ZIKV pathogenesis remains limited (Goellner et al., 2023). In this context, our study focused on ZIKV envelope lipids, investigating the pathogenesis in placental tissues of virions characterized by a different lipid profile. To reach this goal, two viral stocks were obtained through propagation of a ZIKV strain, in virus susceptible cells able to guarantee an extreme different lipid profile such as mammalian Vero cells and mosquito C6/36 cell lines, as previously done for DENV (Hitakarun et al., 2022). To confirm the effective modulation of ZIKV lipid profile, after purification, viral stocks were analyzed by lipidomic. Then, we explored the replication of the viral stocks in immortalized placental cell lines representative of placental tissues in both early and late gestational stages, and on *ex-vivo* cultures of human full-term placental tissue.

2. Methods

2.1. Cell lines

Vero African green monkey kidney (Vero, CCL-81™; ATCC®) cells were grown and maintained in Eagle Minimal Essential Medium (MEM; Gibco, Life Technology) supplemented with 10 % fetal calf serum (FCS; Corning, Sigma-Aldrich) at 37 °C with 5 % CO_2. *Aedes albopictus* mosquito C6/36 (C6/36, CRL-1660, ATCC®) cells were grown and maintained in MEM supplemented with 1mM sodium pyruvate (Sigma-Aldrich), 1 %, 100X non-essential amino acids (MP Biomedicals), 2mM L-glutamine (Gibco™, Life Technology), and 10 % FCS, at 28 °C with 5 % CO_2. Immortalized, human extravillous trophoblast cells (HTR-8/SVneo, CRL-3271™; ATCC®) were grown and maintained in RPMI 1640 medium (RPMI) supplemented with 5 % FCS, at 37 °C with 5 % CO_2. Human villous trophoblast BeWo cells (BeWo, CCL-98™; ATCC®) were grown and maintained in F12K Kaighn's modified medium supplemented with 10 % FCS, at 37 °C with 5 % CO_2. All media were completed with penicillin 100 U/ml (Gibco, Life Technology) and streptomycin 100 µg/ml (Gibco, Life Technology) (1 % P/S). All cells used tested negative for *Mycoplasma sp*. BeWo cells syncytialization was carried out by supplementing the maintainance medium with 10µM forskolin (Sigma-Aldrich) suspended in DMSO (Sigma-Aldrich), for 48 hours. BeWo cells syncytialization was assessed morphologically through an optic microscope and by measurement of β human chorionic gonadotropin (β–hCG) level in the supernatant using a hCG+ β enzyme-linked immunosorbent assay (ELISA) (IBL International). For viral phenotyping, syncitialized BeWo (Sync-BeWo) cells were plated on 24 or 96 well plates pre-coated with collagen type 1 solution (Sigma-Aldrich) diluted 1:3 in sterile water.

2.2. Virus propagation and titration

In this study, we used three different ZIKV strains. An African strain MR766 (ZK-MR; 001v-EVA143) isolated in mice from a *Macaca mulatta* in Uganda in 1947 and passaged five times in Vero cells at the Aix-Marseille University (AMU Laboratory) prior to our acquisition. Two Asian strains, H/PF/2013 (ZK-FP; 001V-EVA1545) isolated from a human serum in French Polynesia in 2013 and ZIKV/Homo sapiens/Honduras/R103451/2015 (ZK-HON; NR-50,355) isolated from human placenta in Honduras in 2016 and obtained after passages in Vero cells. ZK-MR and ZK-FP were purchased by the European Virus Archive goes Global (EVAg) platform, ZK-HON was provided by the Biodefense and Emerging Infections Research Resources Repository (BEI Resources-NIAID). ZIKV strains were propagated in Vero and in C6/36 cell lines at 70 % confluence, using a multiplicity of infection (MOI) of 0.1 and 0.5 respectively, upon a 1-hour adsorption. In Vero cells, the supernatant was harvested at 3 days post infection (DPI) when approximately 60 % of cytopathic effect (CPE) was observed, whereas in C6/36 cells the supernatant was collected at 5 DPI without CPE. Culture supernatants were clarified by centrifugation at 3000 × g for 30 mins at 4 °C to remove cell debris, divided into aliquots and stored at -80 °C until use. Viral stocks obtained from propagation in Vero and C6/36 cells were respectively identified as HON-V, FP-V, MR-V and HON-C6, FP-C6, MR-C6, respectively. Each viral stock was titrated in Vero cells by the focus forming assay (FFA) and the titer expressed as focus forming unit (FFU). The same assay was used to measure the infectivity of tissue culture and explants supernatants. Briefly, 135,000 cell/cm^2 were plated in 96-well plates and cultured at 37 °C, 5 % CO_2. After 24 hours, cells were washed twice with warm phosphate buffered saline (PBS) and incubated at 37 °C in 5 % CO_2 with 50 µl viruses serially diluted in RPMI with 2 % FCS. After 1 hour incubation, a low viscosity overlay medium was added to the cells as described by Matrosovich et al. (Matrosovich et al., 2006). At 48 HPI, inoculum and overlay medium were removed and cells were fixed with 10 % formalin solution at 4 °C. After 30 mins, cells were washed three times with cold PBS and permeabilized with a solution of 0.01 % Triton X-100 (Sigma-Aldrich) for 10 mins at RT. Primary anti-flavivirus antibody 4G2 (Millipore Catalog No. MAB10216) were diluted 1:10,000 in a blocking buffer solution (BB) made with 0.1 % Tween 20 (Sigma-Aldrich), 1 %w/v bovine albumin (Sigma-Aldrich) and PBS. After 1 hour incubation with antibody solution, cells were washed three times with a PBS solution containing 0.05 % Tween-20 (PBS-Tween) and incubated for 1 hour at RT with a peroxidase-conjugated goat anti-mouse IgG (H+L) antibody (Jackson Immuno Research Laboratories) diluted 1:1000 in BB. After five washes with PBS-Tween, revelation was performed incubating cells with the True Blue™ (KPL) peroxidase substrate for 10 mins at RT. The reaction was stopped replacing true blue with distilled water. Virus titer was expressed as FFU/ml.

2.3. Whole genome sequencing

Total RNA was isolated from 140 µl of the ZIKV stocks propagated either in Vero or in C6/36 cells using the QIAamp Viral RNA mini kit (Qiagen) according to the manufacturer's instructions. Whole ZIKA genome was amplified using primers targeting overlapping regions (Table S1) with the SuperScript III One-Step RT-PCR System with High Fidelity Platinum Taq DNA Polymerase (Invitrogen), under the

following cycling conditions: 55 °C for 30 min, 94 °C for 2 min, 40 cycles at 94 °C for 15 sec, 55 °C for 30 sec and 68 °C for 6 min. Amplicons were purified using the Agencourt AMPure XP (Beckman Coulter™), quantified with the Qubit™ dsDNA HS Assay (Invitrogen), and mixed at equimolar concentration. Library preparation was carried out using the Nextera XT DNA library preparation kit and processed on an Illumina MiSeq platform with the MiSeq reagent kit V3 (300-bp paired-end [PE] mode) (Illumina). Raw data were filtered by removing: a) reads with more than 10 % of undetermined ("N") bases; b) reads with more than 100 bases with Q score below 7; c) duplicated paired-end reads. The remaining reads were clipped from Illumina adaptors Nextera XT with scythe v0.991 (https://github.com/vsbuffalo/scythe), cleaned from PCR primers with trimmomatic v0.32 (Bolger et al., 2014) and finally trimmed with sickle v1.33 (https://github.com/najoshi/sickle). Reads shorter than 80 bases or unpaired after previous filters were discarded. High quality reads were aligned against corresponding reference sequence downloaded from Genbank (accession number KX262887.1 for ZK-HON strain, KJ776791.2 for ZK-FP strain, DQ859059.1 for ZK-MR strain) using BWA v0.7.12 (Li and Durbin, 2010) and standard parameters. Alignments were processed with SAMtools v1.6 (Li et al., 2009) for conversion into BAM format e sorting by position. Single nucleotide polymorphisms (SNPs) indicative of the presence of minority variants were called using LoFreq v2.1.2 (Wilm et al., 2012) According to LoFreq usage recommendations, the alignment was first processed with Picard-tools v2.1.0 (http://picard.sourceforge.net) and GATK v3.5 (McKenna et al., 2010, Depristo et al., 2011, Van der Auwera et al., 2013) in order to correct potential errors, realign reads around insertions and deletions (indels) and recalibrate base quality. LoFreq was then run on fixed alignment with option "–call-indels" to produce vcf files containing both SNPs and indels. From the final set of variants, indels were discarded and SNPs with a frequency lower than 1 % or supported by less than 10 reads were filtered out. The 1 % limit is derived from a previous validation generated using synthetic RNA to infer the error rate inherent in library preparation and deep sequencing (data not shown), and is consistent with published work (Wilker et al., 2013, Moncla et al., 2016). Using standard genetic code, nucleotide variants falling into coding regions were transformed into amino acid changes; nucleotide variants within the same codon where manually checked by visual inspection of alignment with IGV (Robinson et al., 2013, Thorvaldsdottir et al., 2013) in order to confirm their independence or, in case, correct their amino acid change. The sequencing data generated in this study is available from SRA under accession number PRJNA729665.

2.4. Sample preparation for lipidomic analysis

To analyze the lipid composition of envelope of ZK-FP strain derived from mammalian (FP-V) and mosquito (FP-C6) cells, highly concentrated and purified ZK-FP stocks were produced in Vero and C6/36 cell lines respectively. Briefly, ZK-FP was propagated in both cell lines as previously described, using ten 182.5 cm^2 T-flasks (CytoOne®). For each cell line, pooled supernatants were clarified at 3000 × g for 30 min at 4 °C, and concentrated by ultracentrifugation in a Sorvall™ MTX 150 Micro-Ultracentrifuge with a T-647.5 Fixed Angle Rotor (Thermo Scientific™) at 150,000 × g for 2.5 hours, at 4 °C. Supernatants were discharged and viral pellets were suspended in 0.5 ml PBS and purified by ultracentrifugation at 116,000 × g for 1.5 h at 4 °C through a discontinuous 10–60 % sucrose gradient, using a TH-641 Swinging Bucket Rotor (Thermo Scientific™). For each stock, visible viral fractions were collected, dialyzed against PBS at 4 °C overnight using Pur-A-Lyzer tubes (Sigma-Aldrich, USA). The viral sample was examined for purity from cellular components using electron microscopy (S1 Fig.) and further concentrated by ultracentrifugation at 150,000 × g for 2.5 hours at 4 °C. Then, the supernatants were discarded and highly concentrated and purified FP-V and FP-C6 viral pellets, each containing 10^6 FFU' were suspended in 0.5 ml of ice-cold methanol (MeOh) and stored at -80 °C until lipid extraction. In order to compare viral envelope composition against the respective cell substrate for propagation, the lipid profile of both Vero and C6/36 cells membranes was determined. For each cell line, 1×10^7 cells were harvested, and centrifuged at 5000 × g. After 20 mins, supernatants were discharged and cells pellets were suspended in 0.5 ml of ice-cold MeOh and stored at -80 °C until lipid extraction. For the extraction, 100μL of viral and cell samples were added of 400uL of chloroform and methyl tert-butyl ether in a 1:1 ratio (CHCl3:MTBE 1:1). The mixture was kept at 4 °C for 1 hour, mixing it every 15 min. After the incubation, the mixture was added of 200μL of H_2O, vortexed, and centrifuged at 15,115 × g for 3 minutes at 4 °C. The lower organic phase was added of 200μL of saturated NaCl solution to obtain the phase inversion. The mixture was vortexed and centrifuged at 15115× g for 3 minutes at 4 °C, and the upper organic phase was pipetted in a glass vial. The procedure was repeated twice for the lipid extraction: on the first mixture, 100μL of MeOH and 400μL CHCl3: MTBE 1:1 were added. The mixture was vortexed and centrifuged at 15,115× g for 3 minutes at 4 °C, and the upper organic layer was pipetted in the glass vial with the first extract. The extracted sample was dried at 40 °C under a nitrogen flow. The dried sample was suspended in 50μL of isopropanol, acetonitrile, and water in a 2:1:1 ratio (IPA: MeCN: H_2O 2:1:1) for the lipidomic analysis in Liquid chromatography–mass spectrometry (LC-MS) and LC-IMMS^E.

2.5. Lipidomics analysis

Untargeted metabolic profiling of samples was performed in positive/negative electrospray ionization (ESI) mode on an Acquity Ultra Performance Liquid Chromatography (UPLC) system (Waters, U.K.) coupled to a Quadrupole Time-of-Flight (QToF) Synapt XS HDMS mass spectrometer (Waters MS Technologies, Ltd., Manchester, U.K.) (S2 Table). The mass range scan was of 20 to 1200 amu, in High resolution MS scan mode. The capillary voltage was set at 0.7KV and the sampling cone voltage at 40 V. The desolvation gas flow was set at 800 L/h with temperature kept at 400 °C. The cone gas flow was set at 20 L/h with temperature kept at 110 °C. To correct for changes in environmental or experimental condition over the course of the analysis, Leucine-Enkephalin solution at a concentration of 100 pg/ml was injected periodically (every 30 s) as internal reference (i.e. lock mass). The analysis was also conducted in Ion Mobility MS^^{E} with a collision ramp from 15 to 55 V to acquire the ions fragmentation patterns and the collision cross section (CCS). The putative lipids classes were identified by our home data base and with the Human Metabolome Database (HMDB https://hmdb.ca)

2.6. Replication fitness in immortalized placenta cell lines

Growth curve experiments were performed to study the replication kinetics of FP-V and FP-C6 in immortalized placental cell lines. HTR-8 and BeWo cells were seeded onto 24-well plates at 135,000 cell/cm2, while Sync-BeWo cells were plated at 140,000 cell/cm^2. After 24 hours, cell monolayers were washed with PBS and incubated with 1 MOI of FP-V and FP-C6, at 37 °C and 5 % CO_2. After 1 hour adsorption, the inoculum was removed and cells were washed three times and replenished with 0.5 ml maintenance medium. Cell supernatants were collected at 0, 6, 24, 48 and 72 HPI, and subsequently stored at -80 °C until titration by the FFA. The experiment was performed three times with four replicates per condition.

2.7. ZIKV infectivity in immortalized placenta cell lines

To compare the infectivity between ZIKV stocks grown in mammalian and mosquito cells, we calculated the median infectious dose (MID) of FP-V and FP-C6 in immortalized placental cell lines. After seeding HTR-8 and BeWo in 96-well plates at 135,000 cell/cm^2, and Sync-BeWo at 140,000 cell/cm^2, cells were incubated at 37 °C in 5 % CO_2. Twenty-

four hours post seeding, cells were washed with warm PBS and incubated with 5-fold dilutions (2×10^5 FFU/50 µl - 2×10^1 FFU/50 µl) of either FP-V or FP-C6 at 37 °C with 5 %CO_2. After 1 hour adsorption, maintenance medium was added, and cell cultures were incubated for five days at 37 °C with 5 % CO_2. Infected cells were fixed and stained, following the same procedure adopted for the FFA. In the presence of multiple infection foci the well was scored as infected. The MID was calculated using the Reed and Muench formula (Reed and Muench, 1938). To evaluate whether the MID values might be affected by the duration of virus-cell incubation as a result of different binding avidities of the two viruses, the same experiment was repeated limiting the incubation times to either 5, 15 or 30 minutes. Each experiment was performed three times, with 6 replicates for each condition.

2.8. ZIKV fusion efficiency in immortalized placenta cell lines

To study the fusion ability of ZIKV with cell endosomes of immortalized placental cells, FP-V and FP-C6 envelopes were labelled with a lipophilic probe able to release fluorescence during lipid mixing. Briefly, FP-V and FP-C6 viral stocks were concentrated, purified through dialysis. Purified viral stocks were inactivated by ultraviolet light (UV) for 60 min as reported by Müller et al. (Müller et al., 2016). To label the viral envelope of FP-V and FP-C6 stocks, Octadecyl rhodamine B (R18; Thermo Fisher Scientific), a self-quenching lipophilic probe was dissolved in ethanol at 10 mg/ml and further diluted in PBS buffer containing 20 mM Hepes and 150 mM NaCl (pH 7.2) to produce a 1 µg/ml R18 stock solution. FP-V and FP-C6 were incubated with the R18 stock solution at a ratio of 1:100 between the ZIKV envelope (E) protein, previously determined through an ELISA test (ELISA, KIT40543; Sino Biological Inc.), and the lipid probe (i.e. 2 ng of viral protein with 200 ng of R18). The incubation occurred on a rocker, for 2 hours at 4 °C. R18-labelled FP-V and FP-C6 were prepared freshly for each fusion experiment. For the fusion assay, HTR-8 and BeWo cells were previously seeded in 96-well plates at 135,000 cell/cm^2, washed once with cold PBS and incubated with 5×10^4 FFU/ml of either of the two R18-labelled viruses, at 4 °C to prevent viral internalization. After 1 hour incubation, viral inoculum was removed and cells washed twice with cold PBS to remove unbound virus. To initiate viral internalization and virus-endosome fusion, cells were rinsed with pre-warmed medium and incubated for 12 mins at 37 °C into a VICTOR Nivo Multimode Microplate Reader spectrofluorometer (Perkin-Elmer; USA). The fusion of the labelled viral envelopes with the cell endosome membranes resulted in the partitioning of the R18 probe caused by lipid mixing, which was accompanied by an increase in fluorescence. R18 fluorescence was monitored at 1 min intervals at 530/30 nm excitation and 570/10 nm emission. Concentrated supernatants of mock-infected Vero and C6/36 cells were used as assay controls. Data were visualized as relative fluorescence units (RFU) and corrected subtracting background fluorescence from control samples. The highest RFU value observed within 12 mins of monitoring was defined as emission peak. The experiment was conducted twice.

2.9. Full-term placenta explant cultures

Healthy human placental tissues were obtained from 3 different full-term elective cesarean deliveries in case of non-labor after 38–40 weeks of gestation at the Department of Women's and Children's Health, University of Padova (Padova, Italy). Procedures were authorized by the Padova University Hospital research ethics committee (n. 0051708/2017). Placentas were collected immediately after the delivery, washed extensively with cold PBS and transported in a RPMI medium complemented with 2 % FCS, 1 % P/S, 10 µM nystatin (Sigma-Aldrich) and 0.1 mg/ml gentamicin sulfate 10 mg/mL (Euroclone) to the Istituto Zooprofilattico Sperimentale delle Venezie (Legnaro, Italy) laboratories. Placentas were separated from decidual and amniotic tissue layers, dissected in three parts and abundantly washed with 1 % P/S to remove blood clots. Explants were obtained by cutting slices of approximately 30-mm^3 from each placental section. Each explant was cultured in a single well in 24-wells plates with completed RPMI medium at 37 °C, in a humidified atmosphere containing 5 % CO_2.

2.10. ZIKV replication fitness and infectivity in human placental explants

Human placental explants were used to compare the replication kinetics of ZIKV strains grown in either mammalian (FP-V, HON-V, MR-V) or mosquito (FP-C6, HON-C6, MR-C6) cell lines. Briefly, four placental explants were washed twice with warm PBS and incubated at 37 °C and 5 % CO_2 with 0.5 ml complete RPMI medium containing 10^5 FFU of each virus. After a 12-hour incubation, explants were washed four times with warm PBS and singularly cultivated in wells with 1.6 ml of complete RPMI medium containing 10 % FCS, 1 % P/S, 0.1 mg/ml gentamycin. At 24, 48, 72 HPI, 150 µl of culture supernatant was collected from each well and stored at -80 °C until viral titration using a quantitative real-time RT-PCR (rRT-PCR). Additionally, we investigated the infectivity of the viruses in full-term placenta by determining the median infectious dose in placental explants (PID_{50}). To evaluate the PID_{50} of each viral stock, five placental explants were washed twice and subsequently incubated with 0.5 ml of 10-fold serially diluted viruses (1×10^5 FFU/0.5 ml - 1×10^1 FFU/0.5 ml) for 12 hours at 37 °C in 5 % CO_2. Following incubation, explanted tissues were washed four times with warm PBS and singularly cultivated with 1.6 ml of complete RPMI medium. Explant supernatants were collected at 0 and 72 HPI and stored at -80 °C until viral detection by quantitative rRT-PCR. A placental explant was considered positive for ZIKV when the viral genomic load in the supernatant collected at 72 HPI was at least five times higher than the one detected at 0 HPI. The fraction of positive/negative explants per dose was used to calculated the PID_{50} of each viral stock using the Reed and Muench formula (Reed and Muench, 1938). The same experimental setting was applied for all of the three collected placentas ($n = 3$).

2.11. Molecular testing by real-time RT-PCR

Real-time RT-PCR was carried out according to the assay developed by Lanciotti et al. (Lanciotti et al., 2008) (Table S1). Briefly, nucleic acids were isolated from 150 µl suspension using the QIAsymphony DSP Virus/Pathogen Midi Kit on a QIAsymphony SP instrument (Qiagen). The amplification reaction was assembled with the QuantiTect Probe RT-PCR Kit (Qiagen), 600 nM each primer, 400 nM probe, 5 µl template and nuclease-free water up to 25 µl. Thermal cycling was carried out on a CFX96 Real-time System (Biorad) at 50 °C for 30 min, 95 °C for 15 min, followed by 40 cycles at 94 °C for 15 sec and 55 °C for 60 sec. For viral genome quantification, standard curves consisting of 10-fold serially diluted in vitro transcribed RNA were included in each run along with the samples. Standard RNA was prepared in house using the MEGAshortscript T7 Transcription Kit and the MEGAclear Kit (Ambion) according to the manufacturer's instructions. The limit of quantification (LoQ) of the assay was preliminarily assessed (10 GC/µl with 43 % CV). Viral load in explant supernatants was determined by interpolation with the calibration curves and expressed as log10 genome copies (GC) per µl of RNA.

2.12. Histology and Immunohistochemistry

To evaluate the tissue integrity and viability of the placental explants, cultured tissues were analyzed by histological and immunohistochemical methods, respectively. For each of the three sampled placentas, five uninfected explants were collected at 24 and 72 hours post cultivation, fixed in 10 % formalin solution for 24 hours and routinely processed for histology by staining 4 µm sections with hematoxylin and eosin (HE). Immunohistochemistry (IHC) was performed on 3 µm sections using the BenchMark ULTRA automated immunostainer (Ventana Medical Systems, Tucson, AZ) to detect the β–hCG antigen, the

glycoprotein hormone synthesized by STB cells. Briefly, the antigen retrieval was carried out using the pre-diluted ULTRA Cell Conditioning (ULTRA CC2) solution (Roche), at 91 °C, and pH 6.0, for 44 minutes. Slides were incubated for 32 minutes at RT with the ready-to-use primary polyclonal anti-β–hCG antibody (Leica) and an ultraView Universal DAB Detection Kit (Roche) was used as detection system. Placental tissues collected immediately after the C-section were used as a reference tissue to evaluate the physiological histological architecture and the expression of β–hCG. P Negative controls were obtained by omitting the primary antibody during the labelling steps to highlight the nonspecific bindings.

2.13. Statistical analysis

The statistical analyses were performed using Prism 9.0 (Graph Pad) software. Ratio paired *t*-test was used for comparison between two groups of normal or log-normal distributed data. One-way ANOVA followed by *post-hoc* test was applied to compare the means of multiple groups. The interval of confidence applied in ratio paired *t*-test ranged from 90 to 99 %, depending on the data set analyzed. Contingency data were analyzed by Fisher's exact test considering significant p values $\leq$ 0.05.

3. Results

3.1. Genetic analysis of ZIKV stocks propagated in mammalian and in insect cell lines

To verify the genetic identity of stocks generated in mammalian and insect cell lines, we conducted an NGS based in-depth comparative analysis of single amino acid polymorphisms (SAPs). This analysis was conducted to assess whether for each virus strain, the two stocks contained similar proportions of the same quasispecies. Since the intrinsic error in the calculation of polymorphism frequency is equal to 1 %, SAPs that differed by less than 2 % in the two viral stocks were not considered in our quasispecies comparison (Wilker et al., 2013, Moncla et al., 2016). Based on these criteria, we identified 14 SAPs for ZK-FP, 6 for ZK-HON, and 24 for ZK-MR (Table S3). For both stocks belonging to ZK-FP, we observed that the amino acid changes had frequencies that did not reach the consensus level of 51 %, ranging between 0.0 and 41.4 %. For this virus, the SAPs fell within the prM ($n = 2$), the E ($n = 3$), the NS1 ($n = 5$) and the NS2B ($n = 4$) and were characterized by a median difference in frequency between FP-V and FP-C of 10.7 % ± 4.1 %. The only SAPs that were found exclusively in either one of the two batches were changes S455L (2.3 %) and M220T (3.2 %) in the E protein of FP-V and in the NS1 of FP-C, respectively. For ZK-HON, we recorded SAPs ranging in frequency from 0 to 56 %, with only one mutation (H401Y) in the E protein reaching the consensus level in the HON-V stock. Moreover, the HON-V stock carried an exclusive change in the E protein (S455T) at a frequency of 2.4 %. For this strain, the SAPs fell within the E protein ($n = 5$) and the NS2A protein ($n = 1$), with a median difference in the frequency between the two stocks of 7.2 % ± 2.9 %. For the ZK-MR viruses, the SAPs ranged in frequency from 0 to 17.6 %. These amino acid changes sit on the proteins prM ($n = 2$), E ($n = 10$), NS2A ($n = 2$), NS2B ($n = 2$), NS3 ($n = 6$), NS5 ($n = 2$) and their median difference in the distribution between the two stock was equal to 3.4 % ± 2.1 %. For this virus, we identified a higher number of mutations that were exclusively present in one of the two stocks. In particular, the MR-V stock had the exclusive mutation I141T (2 %) at the level of the prM protein, A416V (3.1 %) and S449L (3.4 %) in the E protein, A117V (3.1 %) and I118T (2.6 %) in the NS2A protein, the mutation K587T (5 %) in the NS3 protein, and the amino acid change E560G (2.2 %) in the NS5. On the other hand, the MR-C6 stock had the exclusive changes R158S (2.6 %), F192L (2.6 %) and L370M (2.4 %) in the E protein. Few amino acid signatures were shared between the different viruses and the different stocks. In particular the F130L SAP was observed in the prM protein of both stocks of the ZK-FP and the ZK-MR viruses; quasispecies with the S455L mutation in the E protein were observed to be common to ZK-FP and ZK-HON. In the NS2B proteins of both ZK-FP and ZK-MR we observed the same SAP M32I. Notably, for all of these SAPs the frequency was found to be higher in the Vero cell batches than in the C6/36 cell batches.

3.2. Lypidomic analysis of the envelope of ZIKV strains originating from mammalian and insect cell lines

Through lipidomic analysis, we investigated the lipid composition of the envelope of two ZIKV stocks derived from the same virus strain propagated in different cell lines. Mammalian Vero and insect C6/36 cell lines were selected due to their high susceptibility to ZIKV infection. Specifically, C6/36 cells, unlike mammalian cells, do not synthesize cholesterol, theoretically ensuring a distinct range of lipid substrates to the viral assembly (Hafer et al., 2009). In Fig. 1A, the chromatograms show the FP-V and FP-C6 lipid fractions separated by mass along the retention time. As expected, FP-V and FP-C6 exhibited overall different lipid spectra, reflecting the substantial diversity in lipid composition between Vero and C6/36 cell lines (S2 Fig.). However, the spectrum of each viral stock did not overlap with that of the cell line of origin, indicating that the viral envelope retains its distinct lipid profile (S3 Fig.) To underscore the distinction between FP-V and FP-C6 lipid profile, we highlighted the numerous peaks mutually exclusive for each viral stock (Fig. 1B). The characterization of those peaks revealed a higher expression of seven molecules belonging to the phosphatidylcholine (PC) class, and two from the class of the phosphoethanolamines (PEs) in the FP-V stock. In contrast, FP-C6 stock displayed exclusivity in three lipid fractions related to PEs and one to the phosphatidylglycerols (PGs) (Table 1). This finding suggests that the lipid structure of ZIKV envelope may vary depending on the host cell of origin.

3.3. Replication fitness and infectivity in immortalized placental cells of ZIKV strains derived from mammalian and insect cell lines

To evaluate how ZIKV with different lipid profile replicated in immortalized placental cell lines, kinetics of FP-V and FP-C6 viral stocks was assessed in HTR-8 cells, as this cell line is considered a model of invasive extra-villus trophoblast, in BeWo cells representative of CTB cells and in Sync-BeWo cells representative of the STB (S4 Fig.) (Carrera et al., 2021). Growth curves demonstrated that all placental cell lines supported FP-V and FP-C6 replication. At 72 HPI, in HTR-8 and BeWo cells, FP-V and FP-C6 recorded mean viral titers above 7.00 Log10 FFU/ml and 6.5 Log10 FFU/ml respectively (Fig. 2a, b); whereas in Sync-BeWo, FP-V and FP-C6 reached mean viral titers of 6.3 Log10 FFU/ml and 5.4 Log10 FFU/ml respectively (Fig. 2c). The overall replicative fitness of FP-V and FP-C6 was compared for each cell line through the calculation of the area under the curve (AUC) (Fig 2d, e, f). The results indicated that FP-C6 had a significantly lower replication efficiency in villous trophoblast BeWo and Sync-BeWo cells compared to FP-V ($p=0.0095$ and $p=0.0026$). In contrast, no significant difference was observed for FP-V and FP-C6 AUCs in HTR-8. Taken together these data suggest that extravillous trophoblasts are highly permissive to ZIKV regardless of its cellular derivation, while villous trophoblasts sustain a more efficient replication for the mammalian-derived FP-V.

To better characterize the viral fitness of ZIKV stocks in trophoblast cells, the MID of FP-V and FP-C6, was determined in the three immortalized placental cell lines as a measurement of viral infectivity. At first, we facilitated ZIKV infection leaving viral inoculum for 5 days on the cell substrates, following a similar approach to common virologic isolation and titration protocols for this virus. Under this condition, in BeWo cells, the FP-V and FP-C6 viruses recorded MID values of 38.06 FFU/50μl and 339.13 FFU/50 μl, respectively (Fig. 2h). For the same incubation time, in Sync-BeWo, the FP-V and the FP-C6 scored MID values of 3,025.79 FFU/50μl and 327,470.78 FFU/50 μl, respectively

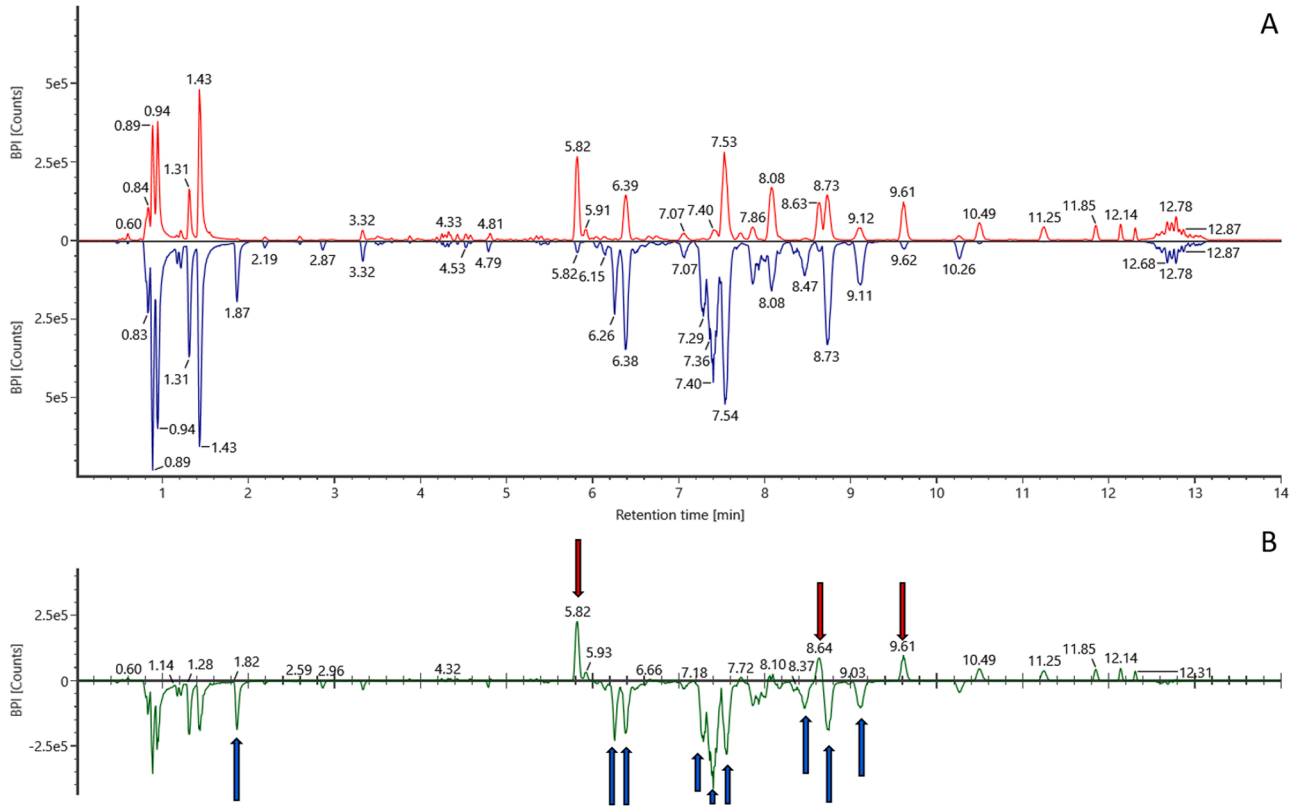

Fig 1. Chromatograms in positive mode of lipid fractions expressed in ZIKV strains envelope. (A) In red the chromatogram of lipid fractions expressed in ZIKV stock derived from C6/36 mosquito cells (FP-C6); in blue, the chromatogram of ZIKV stock originated from Vero mammalian cell line (FP-V). (B) In green the chromatogram resulting from the difference between FP-C6 and FP-V chromatograms. The red and blue arrows indicated the lipid fractions highly expressed in FP-C6 and FP-V respectively.

Table 1
Lipid molecules mutually exclusive of each viral stocks envelope. For the mammalian-derived FP-V stock and mosquito-derived FP-C6 stock, the table reported the lipid molecules mostly expressed, their retention time and the lipid class of belonging.

ZIKV stocks	Putative molecole	Retention time	Lipid class
FP-V	PC (O-14:0_2:0)	1,79	Phosphatidylcholine
	PC (16:0_16:1)	6,38	
	PC (16:0_18:3)	7,29	
	PC (16:0_18:1)	7,42	
	PC (18:0_22:4)	7,57	
	PC (18:0_18:1)	8,47	
	PC (O-18:0_18:1)	9,10	
	PE (18:3_20:0)	6,26	Phosphoethanolamines
	PE (18:0_18:1)	8,76	
FP-C6	PG (16:0_18:0)	8,64	Phosphatidylglycerols
	PE (12:0_20:2)	6,26	Phosphoethanolamines
	PE (16:1_22:0)	9,70	

(Fig. 2i). For both BeWo and Sync-BeWo, we observed approximately a 8.9 fold-change between the MID values of mammalian and insect cell derived batches, and these differences were found to be statistically significant (p=0.0061and p=0.0006). In contrast, at the same time point, FP-V and FP-C6 displayed a similar infectivity in HTR-8 cell with a MID value of 379.95 FFU/50 µl and 513.48 FFU/50 µl, respectively, which did not result in a statistical significance (Fig. 2g). Moreover, we investigated whether a limitation in the virus-cell incubation time could affect infectivity. As expected, the decrease of contact time from 5 days to 5 mins affected viral infectivity, leading to an increase in the MID for both ZIKV stocks, in all of the tested placental cell lines (Fig. 2 g, h, i and Table S4). However, a reduction in the contact time did not alter the ratio between the MIDs of FP-C6 and FP-V, which resulted statistically comparable among different time points in each placental cell line (S5 Fig.). Collectively, these assays indicate that the mammalian cell-derived ZIKV lot requires a lower dose to infect villous trophoblasts than the insect-cell-derived lot; however limiting the cell-virus incubation time did not consistently enhance the advantage of FP-V over FP-C6 across all tested cell lines.

3.4. ZIKV strains fusion efficiency in immortalized placenta cell lines

We investigated the capacity of uncoating between FP-V and FP-C6 through a fusion assay using lipophilic R18 molecules. R18 works as a self-quenching molecule, releasing fluorescence when the concentrated dye labelling in the viral envelope is fractioned and dispersed by fusion with the host membrane lipids (Nour et al., 2013). In HTR-8 cells, the fluorescence spectra shared a similar pattern between the two ZIKV viral stocks: FP-V displayed the highest RFU value after 1 min of incubation, while FP-C6 fluorescence peak was recorded one minute later (Fig. 3). In contrast, in BeWo cells, FP-C6 displayed a relatively flat spectrum with the highest emission peak at 6 mins, while the FP-V rapidly reached its emission peak around at 1 min post incubation. These data demonstrated that FP-C6 did not rapidly fuse its envelope with the endosome membranes of the Bewo cells, displaying a considerable delay with respect to FP-V.

3.5. Infectivity and replication kinetics of ZIKV stocks derived from mammalian and insect cell lines in human full-term placental explants

To further test whether the cell-origin of the viral envelope might affect the infectivity and replication fitness of ZIKV in villous trophoblasts, explants of full-term placentas were infected with three different ZIKV strains cultivated in mammalian Vero (FP-V, HN-V, MR-V) and

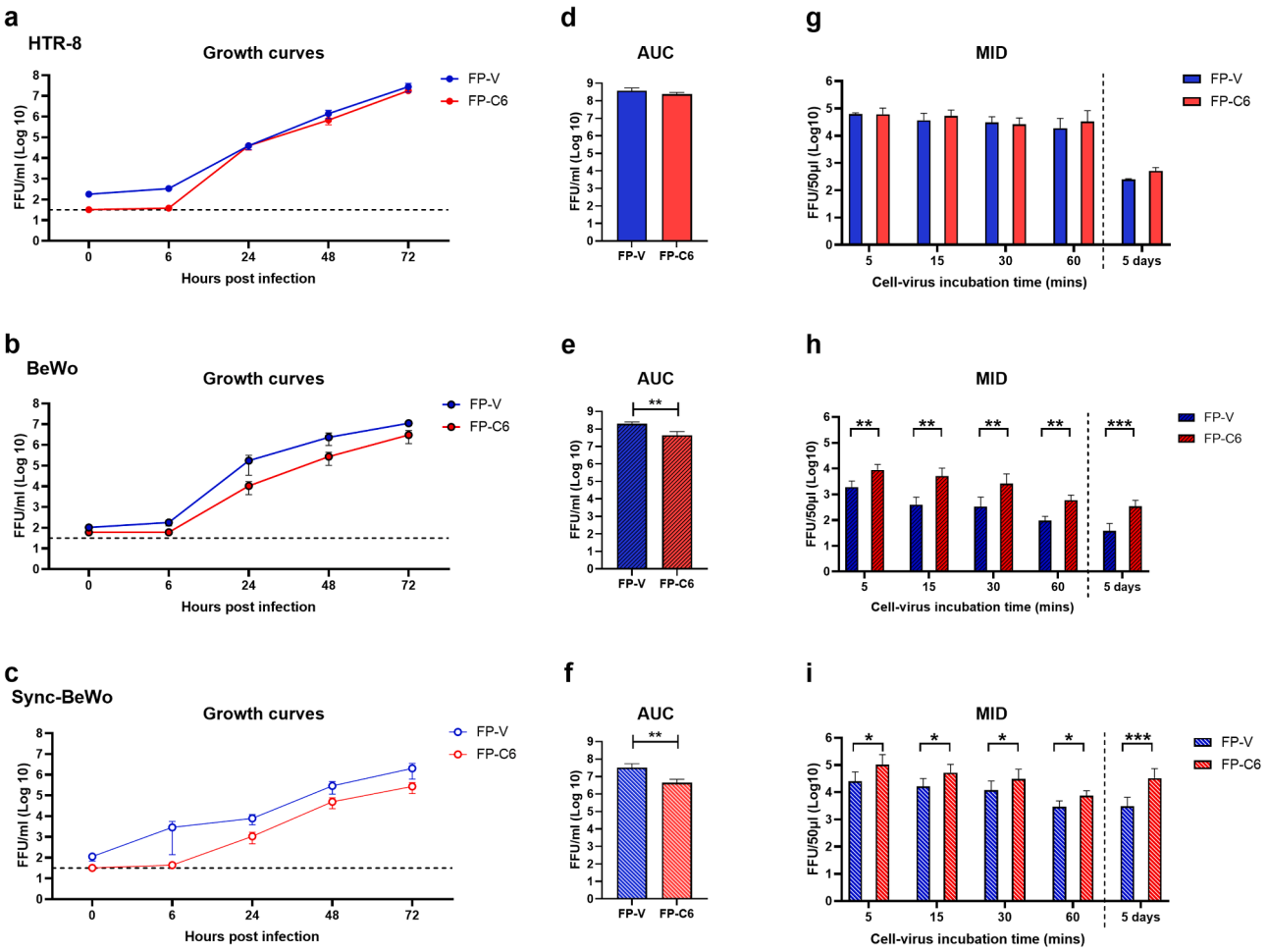

Fig. 2. Growth curves, area under the curve and mean infectious dose (MID) of ZIKV strains derived from mammalian and mosquito cell lines in immortalized placental cell lines. Growth curves (GC) of ZIKV derived from mammalian Vero cell lines (FP-V) in blue, and ZIKV originated from mosquito C6/36 cell lines (FP-C6) in red, on immortalized extravillous trophoblast (HTR-8) (a), villous trophoblast (BeWo) (b) and syncytiotrophoblast (Sync-BeWo) (c). The black dashed-line indicates the assay limited of quantification (LoQ = 66 PFU/ml). Area under the curve (AUC) of FP-V (in red) and FP-C6 (in blue) growth curves were reported in HTR-8 (d), BeWo (e) and Sync-BeWo (f) cell lines. The GC and AUC graphs show mean and standard error (SEM) from at least three independent experiments. AUC statistical significance was calculated using a ratio paired t test with 99 % interval of confidence with *, $p \leq 0.01$; **; $p \leq 0.001$;***, $p \leq 0.0001$. MID of ZIKV derived from FP-V (in blue), and FP-C6 (in red) on HTR-8 (g), BeWo (h) and Sync-BeWo (i), presented as means with SEM from at least three independent experiments. Statistical significance was calculated after data log-normalization using a ratio paired t test with 90 % interval of confidence with *, $p \leq 0.1$; **; $p \leq 0.01$;***, $p \leq 0.001$.

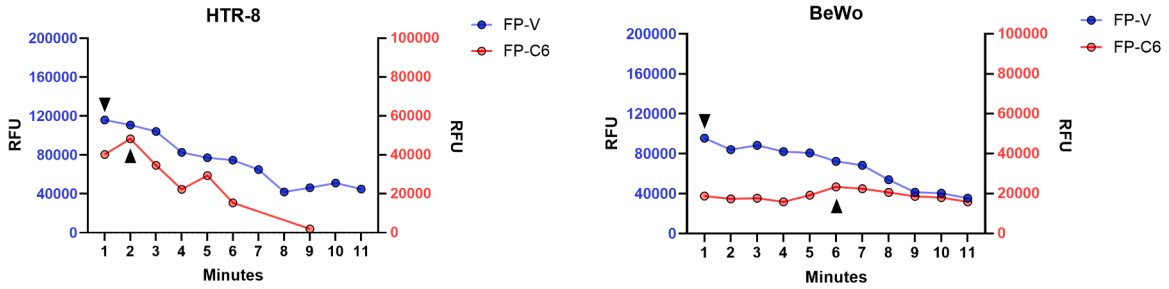

Fig. 3. Fusion efficiency of ZIKV strains derived from mammalian and mosquito cell lines in immortalized placental cell lines. The lipid envelope of UV-inactivated ZIKV derived from mammalian Vero cell lines (FP-V) in blue, and ZIKV originated from mosquito C6/36 cell lines (FP-C6) in red, were labelled with Octadecyl rhodamine B (R18) a lipophilic, self-quenching fluorophore. (On the left) The immortalized extravillous trophoblasts (HTR-8), and (on the right) villous trophoblasts (BeWo) were incubated for 1 hours at 4 °C with R18 labelled ZIKV strains using a MOI of 0.01. After two washes to remove viral inoculum, cells were incubated with pre-warmed medium in a fluorimeter set at 37 °C. The fusion of labelled envelope of FP-V (blue) and FP-C6 (red) with placental cell endosomes, caused R18 self-quencing, which was detectable as fluorescence spectrum by fluorimeter. Fluorescence of both FP-V and FP-C6 was expressed as relative fluorescence units (RFU) and presented as median of two experiments. For each time point, RFU were calculated subtracting background fluorescence of non-infected cells from fluorescence of cells incubated with UV ZIKV strains.

insect C6/36 (FP-C6, HN-C6, MR-C6) cell lines. Prior to the infection, explanted villi displayed a histologically unaltered tissue and STB cells actively secreted β-hCG confirming their viability (S6 Fig). Notably, our findings show that irrespective of the ZIKV lineage and of the time of supernatant collection, viruses originating from Vero cells successfully established an infection in all placental explants collected from three different placentas. In contrast, the C6/36-derived stocks infected a significantly lower percentage of explants, recording 42 % infection rate for FP-C6 (p=0.0017), 25 % for HON-C6 (p=0.0001) and 50 % for MR-C6 (p=0.0047) at 72 HPI (Fig. 4 a, b, c). Consistent with these observations, all ZIKV strains of mammalian cell derivation recorded a significantly lower PID_{50} than isolates of mosquito cell origin (FP p=0.013, HON p=0.031 and MR p=0.004), an outcome considered as indicative of a higher infectivity of these strains in placental tissues collected during the third trimester of pregnancy (Fig. 4d, e, f). In particular, Vero cell-derived strains showed 6.4, 27.0 and 148.6 times higher infectivity than their mosquito-derived batches for the ZK-FP, ZK-HON and ZK-MR viruses, respectively.

4. Discussion

Among flaviviruses, ZIKV is the only pathogen officially recognized as a teratogenic agent, because of its ability to infect and cross the placental barrier causing the impairment of fetal neuronal developments

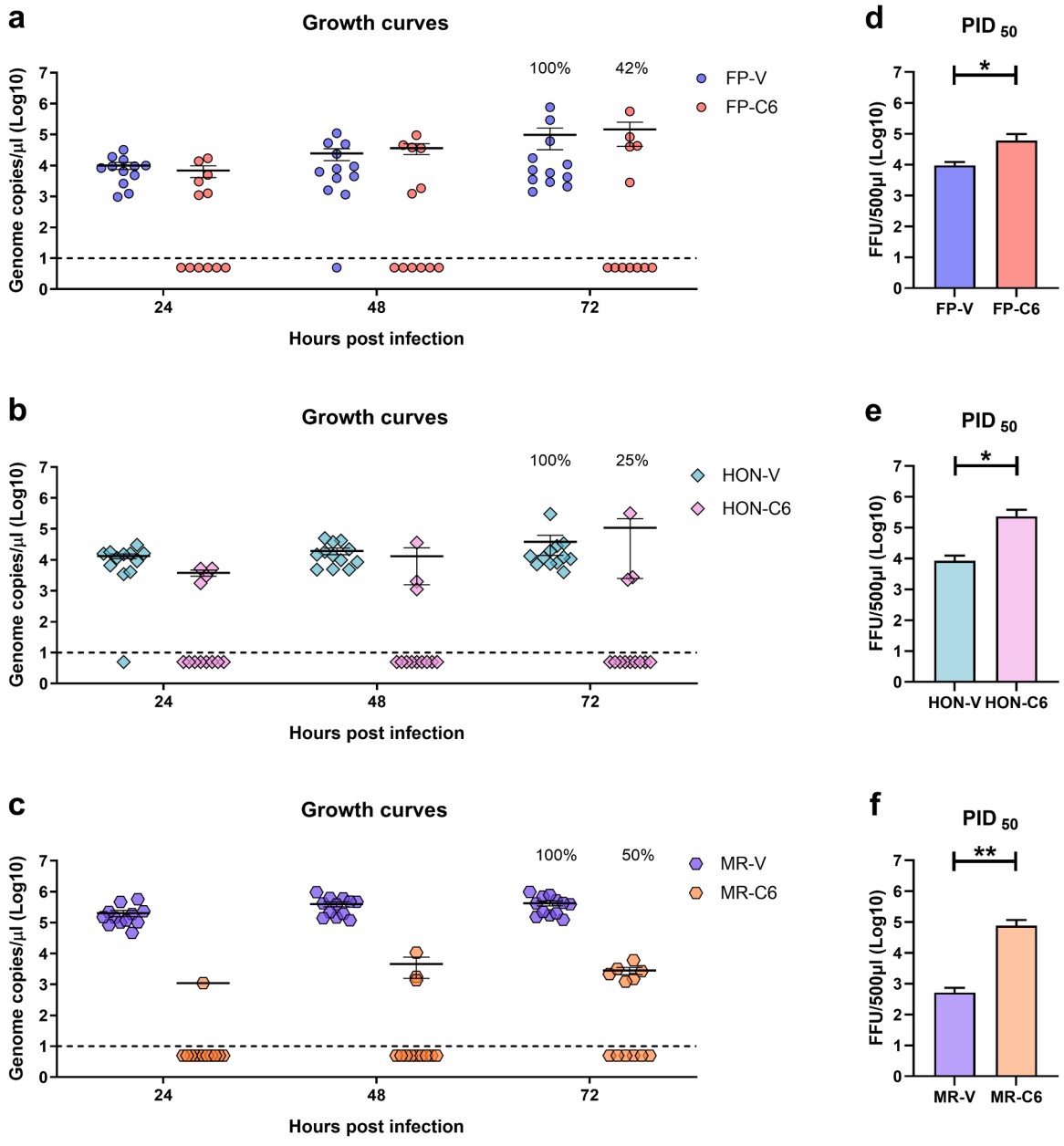

Fig. 4. Replicative kinetics and placenta mean infectious dose 50 (PID_{50}) of ZIKV strains derived from mammalian and mosquito cell lines in human full-term placental explants. (a, b, c) The replicative kinetics of ZIKV derived from mammalian Vero cell lines (FP-V, HN-V, MR-V), and ZIKV originated from mosquito C6/36 cell lines (FP-C6, HN-C6, MR-C6), on placental explants from full-term elective cesarean deliveries. Results display viral loads of single explants expressed as log10 GC/µl RNA. Mean values and standard errors (SEM) were calculated based on ZIKV positive explants from three independent experiments. The black dashed-line indicate the qRT-PCR limited of quantification (LoQ=10 genome copies). For graphical purposes, negative explants were arbitrarily given a value of 5 GC/µl RNA. (d, e, f) PID_{50} of mammalian cell derived FP-V, HN-V, MR-V and mosquito cell derived FP-C6, HN-C6, MR-C6 in placental explants from full-term elective cesarean deliveries. Results were presented as means and SEM from at least three independent experiments. Statistical significance was calculated using a ratio paired t test with 90 % interval of confidence with *, $p \leq 0.1$; **; $p \leq 0.01$; ***, $p \leq 0.00$.

described as CZS (CB Coyne and Lazear, 2016). Women infected with ZIKV in the first trimester of pregnancy reported a higher rate of CZS than those infected in the second or third trimester, when placental cells constituting the STB increase their interferon-dependent resistance to viral infections (Ades et al., 2021). However, ZIKV is able to directly, or indirectly, impair fetal development also at late stages in pregnancy (Nielsen-Saines et al., 2019). Numerous studies investigated the pathogenic mechanisms underpinning the ability of this virus to bypass a fully developed placental barrier. Nonetheless, at the time of writing, scholars have largely ignored the hypothesis that viral and host lipids might play a bigger role in the crossing of the placenta (Villalobos-Sánchez et al., 2022).

Over the last decade, there has been increasing research into the role of lipids in the pathogenesis of flaviviruses (Leier et al., 2020, Chen et al., 2020). However, most of this work has focused on ZIKV's ability to alter the host cell lipid machinery, without delving deeper into the function of viral lipids in host cell infection (Martín-Acebes et al., 2016). In this study, we hypothesized that viral lipids could be a potential determinant of ZIKV pathogenesis at the level of mother-fetus interface during the last stage of pregnancy. Consequently, we investigated viral replication of two ZIKV stocks different for the envelope lipid composition in human placental *in-vitro* models. For this purpose, we generated a pair of viral stocks, propagating the French Polynesian ZIKV isolate in either a mammalian Vero cell line (FP-V) or a mosquito C6/36 (FP-C6) cell line and evaluated their phenotype in terms of infectivity, using immortalized placental cell lines and placental explants. Importantly, we used both mammalian and insect cell lines to obtain our ZIKV stocks, as the C6/36 cell line's inability to produce cholesterol, along with its distinct membrane lipid composition compared to mammalian cells, ensured that the resulting virions had a unique lipid profile (Hitakarun et al., 2022, Hafer et al., 2009). When FP-V and FP-C6 stocks were used to infect human placental cell lines, we observed that irrespective of the line, both stocks replicated to high titers as previously demonstrated by Carrera and colleagues (Carrera et al., 2021). Notably, in our study, villous cytotrophoblasts and syncytiotrophoblasts cell lines like BeWo and Sync-BeWo proved to be more permissive to the FP-V compare to FP-C6. Furthermore, the higher replication fitness of the FP-V stock paired with an 8.9-fold higher infectivity of this strain in the same cell lines as indicated by the different MID values. In contrast, in the HTR-8 extravillous invasive trophoblast cell line, FP-V and FP-C6 showed similar replication and infectivity, suggesting that susceptibility to viruses of different host cell origin might be cell type specific, even within the same tissue. Interestingly, Bayer and colleagues observed a similar pattern in an analogous experimental setting where the phenotype of two distinct ZIKV isolates, propagated in Vero and C6/36 lines respectively, were investigated in immortalized placental cells. (A Bayer et al., 2017). Indeed, authors determined that the Vero-grown stock achieved a significantly higher percentage of ZIKV-infected cells than the C6/36-grown stock in cells representative of the villous trophoblast, while a negligible difference between the strains was observed in the HTR-8 cells.

To further investigate FP-V and FP-C6 phenotype, we studied the replicative pattern of Vero and C6–36-derived ZIKV stocks in explanted villi from term placental tissues obtained after birth through cesarian sections. In this experiment, we noticed that when an infection was established, FP-V and FP-C6 showed a similar replicative kinetics with comparable viral titers; however, the FP-C6 virus displayed a significantly lower infection rate, replicating in less than half of the total explants. To exclude that this cell origin-dependent phenotype was a unique characteristic of the French Polynesia strain, we performed the same experiment using two additional ZIKV strains, namely ZK-HON and ZK-MR. Interestingly, the same pattern emerged, confirming that the viruses derived from Vero cells increased in infectivity when compared to their mosquito cell-derived counterparts. Collectively, our phenotypic characterization indicate that stocks with a higher fitness in term placental explants and in cell lines representative of the CTB and STB share a Vero cell-origin.

Having confirmed the higher infectivity of ZIKV stocks derived from Vero cell in trophoblast cells, we further investigated the pathogenic mechanism, focusing on a single strain, ZK-FP, as this strain is more representative of the main circulating lineage compared to ZK-MR, and is the ancestor of ZK-HON (Assis et al., 2020). Firstly, we assessed both viral attachment and entry into host cells, evaluating the infectivity of FP-V and FP-C6 by limiting the adsorption time of viral particles to immortalized placental cells, as the restriction of either virus-receptor contact time or receptor density are both common approaches in virology to assess receptor affinity (Guo et al., 2018). As expected, our results showed that a shorter adsorption time requires a higher viral dose to infect cells. However, regardless of the incubation time, the difference in infectivity between FP-V and FP-C6 remained consistent with that previously reported in MID experiments with 5-day incubation times across all placental cell lines. These data indicated that the different infectivity of FP-V and FP-C6 was not determined by an advantage of one viral stock over the other in viral attachment or entry into the host cells. Beside viral entry, another aspect able to influence viral infectivity is the efficiency of viral and endosome membrane fusion, necessary to release the viral genome into the host cell cytoplasm (Agrelli et al., 2019). In this study, we investigated the fusion activity of FP-V and FP-C6 in immortalized placental cell lines using a R18 fluorophore. Our results showed that, in HTR-8 cells, FP-V and FP-C6 reached the maximum fusion activity by two mins post viral entry, consistent with the fusion kinetics of other flaviviruses (Nour et al., 2013, van der Schaar et al., 2008). However, in BeWo cells, the fusion behavior of the two viral stocks greatly differed, with FP-C6 exhibiting a substantial delay in the fluorescence emission peak compared to FP-V. Regardless of the cell line tested, FP-V exhibited higher fluorescence levels compared to FP-C6; however, this was likely due to the differential incorporation of the R18 probe, which is lipid-dependent (Buranda et al., 2010). Our findings suggest that the differential fusion ability of FP-V and FP-C6 stocks was the key factor which most likely determined the different infectivity and replication fitness in villous trophoblasts.

Interestingly, the fusion phase was mainly determined by efficiency of both viral and host membrane lipid interaction (Martín-Acebes et al., 2016, Zaitseva et al., 2010, Ripa et al., 2021). Indeed, besides proteins and pH, different compartment-specific lipids are required for fusion of flaviviruses such as DENV, Japanese encephalitis virus and YFV (Zaitseva et al., 2010, Nour et al., 2013). Moreover, it has been shown that changes in the lipid composition of the viral membrane can impair the fusion step of flaviviruses (Osuna-Ramos et al., 2018). Furthermore, Goellner and colleagues recently demonstrated that a low cholesterol level in the host target membrane triggers the premature fusion of ZIKV, affecting viral infection and replication (Goellner et al., 2023). These evidences point to viral lipids, rather than the genome or proteins, as being responsible for the differing in fusion activity of ZIKV stocks in villous trophoblasts. In mechanistic terms, it could be possible that the lack or enrichment of certain lipid classes on ZIKV stocks envelope could have affected the physical-chemical properties of viral membrane curvatures and fluidity, influencing the efficiency of viral fusion and consequently its infectivity (Joardar et al., 2022). Interestingly, the lipidomic analysis conducted on viral stocks revealed a higher enrichment in lipids for the mammalian-derived virus, with phosphatidylcholine being the dominant class. Phosphatidylcholine accounts for the greater percentage of the total lipids in DENV and WNV membranes, suggesting its essential role for an effective flavivirus biogenesis (Hitakarun et al., 2022, Martin-Acebes et al., 2014). Indeed, the cylindrical geometry of phosphatidylcholine provides stability and symmetry to the viral membrane, favoring biophysical robustness, as previously attributed to the DENV membrane in a computational study performed by Reddy and Samson (Reddy and Sansom, 2016). Conversely, lipids exclusive to the insect-derived virions belonged to phosphoethanolamines and phosphatidylglycerols classes. While phosphatidylglycerol confers to the membrane properties that are similar to the ones

associated to phosphatidylcholine, phosphoethanolamine with its inverted conical form introduces a negative curvature, potentially contributing to an increase in the fluidity of the lipid leaflets in the viral envelope (Vial et al., 2021). Collectively, these differences in envelope composition may have influenced the physical interaction between the ZIKV envelope and host cell membranes, leading to either enhanced or reduced fusion efficiency, and consequently affecting infection in both in-vitro and ex-vivo models of villous trophoblasts. Conversely, this assumption was not validated for HTR-8 cells which were not significantly affected by the different envelope composition or viral stocks origin, as demonstrated by results from the fusion assay, the overall replication fitness during multi-cycle infection experiments and the calculation of the MID value. We speculate that in a less permissive environment like the one posed by the CTB and STB and represented by BeWo and Sync-BeWo cells, changes in the envelope composition might be more decisive to establish an infection. On the contrary, invasive cytotrophoblast cells, represented by the HTR-8 cell line, could better accommodate these changes in lipid composition due to their unique lipid rafts which support their migratory and invasive properties (Rashid-Doubell et al., 2007). Interestingly, the pattern of susceptibility of BeWo and Sync-BeWo cells to envelope composition was the same observed in term placental explants, which are characterized by a virtual absence of invasive trophoblast and are rich in STB, suggesting that the phenotype observed *in-vitro* is consistent with what we observed *ex-vivo* in a more complex and highly translational model of the human placenta (Knöfler and Pollheimer, 2013). Overall, our findings support the potential role of viral lipids in determining ZIKV infectivity during later stages of pregnancy.

Our study has several limitations. For our scopes, an ideal comparative experimental setting would have encompassed the use of reverse genetics-engineered genetically identical viruses with distinct lipid composition at the level of envelope, but the technology and know-how to achieve this condition were not yet available at the time of the conceptualization of this study (Atieh et al., 2017). Hence, we tested stocks that were extremely similar in terms of quasispecies composition, although not identical. For this reason, we can't exclude that the presence of a limited number of amino acid polymorphisms in several proteins might have influenced the outcome of our assays. However, these polymorphisms displayed low frequencies constituting minority variants in the almost totality of cases and differing minimally between the two stocks. In particular, for the French Polynesian strain used for the majority of our assays, only two changes were exclusively found in the Vero-derived stock, and their frequency ranged between 2–3 %. Moreover, our findings indicate that ZIKV derived from mosquito cell lines exhibits a lower infectivity rate, but not replication capacity, in villous trophoblast cells compared to ZIKV derived from mammalian cell lines. We propose that this reduced infectivity is likely due to a delayed fusion process of the mosquito-derived virus into the host cell endosome. Consequently, we should focus on mutations in proteins involved in fusion and uncoating processes, such as prM and E (Carbaugh et al., 2019). This limitation further reduces the number of mutations that could play a role in affecting infectivity, thereby minimizing the likelihood that genetic factors account for the phenotypic differences between ZIKV stocks. Furthermore, ZIKV, as most of arboviruses, is considered in a state of evolutionary stasis, determined by predominant purifying selection that support the viral fitness in vertebrate and invertebrate hosts cycling (Riemersma et al., 2021). Consequently, ZIKV has proved to remain highly genetically conserved in nature (Ciota and Kramer, 2010). Finally, in our work, the dramatic difference in the infectivity of Vero cell and C6/36 cell-derived stocks in placental explants was a common trait to three divergent strains, irrespective of the number of polymorphisms. An additional factor that was not taken into account in our study is the influence of protein glycosylation. In insect cells, protein glycosylation is simpler than in vertebrate systems, potentially affecting the recognition of ZIKV envelope proteins by host receptors and impairing the first stages of host cell infection (Glycosylation 2019). However, in our study, the two ZIKV stocks did not differ in their capacity to bind to or enter host cells. Therefore, we believe that glycosylation plays a marginal role in the differentiation of the FP-V and FP-C6 phenotypes. Lastly, we used two immortalized cell lines (Vero and C6/36) to modulate the ZIKV lipidome and generated two viral stocks with differing lipid compositions in their envelopes. However, we aware that the lipid composition of ZIKV virions in real-world scenarios depends on the human tissues in which the virus replicates. Consequently, the lipid structure of a virus reaching placental tissues would originate from previously infected maternal cells. Nonetheless, our experimental model serves as a proof of concept, highlighting the need to focus more on the lipid aspects of ZIKV pathogenesis at the maternal-fetal interface. For this reason, we did not further detail the specific lipid classes, proportions, or their interactions with envelope proteins in FP-V and FP-C6. Instead, we encourage conducting lipidomic analyses on viral samples obtained from clinical specimens to fully elucidate the role of lipids in ZIKV pathogenesis in late stages of pregnancy.

5. Conclusions

Our study provides an original investigation into the impact of cell origin on the lipid composition of the ZIKV envelope and its effect on viral fitness at the level of placental cells. Findings from our *in-vitro* experiments suggest that the interplay between host and viral lipids modulate viral uncoating during the early stages of the replicative cycle in villous trophoblast. As a result, a specific lipid composition of the viral envelope may enhance or diminish the fusion efficiency with the target membrane, influencing the success of the virus genetic release into the cytoplasm and the subsequent initiation of replication. This should be considered during experimental design, as studies on ZIKV pathogenesis in the literature often utilize viruses derived from Vero or C6/36 cell lines indiscriminately, without accounting for the potential impact of the viral cell origin on ZIKV infectivity in specific tissue cells (Chen et al., 2020, A Bayer et al., 2017, Platt, 2018, Hermanns et al., 2018). However, further studies are necessary to characterize the lipids of ZIKV envelope and elucidate their biophysical role at the level of host cell interface.

CRediT authorship contribution statement

Eva Mazzetto: Writing – original draft, Visualization, Methodology, Investigation, Formal analysis, Data curation, Conceptualization. **Alessio Bortolami:** Investigation, Data curation. **Davide Bovo:** Methodology. **Matteo Stocchero:** Formal analysis. **Elisa Mazzacan:** Investigation. **Alessandra Napolitan:** Investigation, Formal analysis. **Valentina Panzarin:** Writing – review & editing. **Maria Rosa Tran:** Investigation. **Gianpiero Zamperin:** Formal analysis. **Adelaide Milani:** Data curation. **Andrea Fortin:** Investigation. **Michela Bigolaro:** Investigation. **Paola Pirillo:** Investigation. **Matteo Pagliari:** Writing – review & editing, Data curation. **Claudia Zanardello:** Writing – review & editing. **Giuseppe Giordano:** Methodology. **Maria Teresa Gervasi:** Resources. **Eugenio Baraldi:** Writing – review & editing. **Calogero Terregino:** Writing – review & editing. **Carlo Giaquinto:** Resources, Project administration, Funding acquisition. **Francesco Bonfante:** Writing – review & editing, Supervision, Project administration, Investigation, Funding acquisition, Conceptualization.

Declaration of competing interest

The authors declare that they have no known competing financial interests or personal relationships that could have appeared to influence the work reported in this paper.

Acknowledgments

The authors thank the PENTA Foundation team for their support during the entire project. We gratefully acknowledge the assistance of the entire health care team from Padua hospitals, who collaborated in providing placental samples for the *ex-vivo* study. We are especially grateful to the pregnant women who decided to donate their full-term placenta for research purposes. We also thank all the technician staff at IZSVe, in particular Daniele Facco, Silvia Maniero, Elena Bertoli, Sonia Fassina, and Erika Melchiotti for their invaluable contribution in the laboratory.

Funding

This project has received funding from the European Union's Horizon 2020 research and innovation programme under grant agreement No 734857, ZIKAction Project.

Supplementary materials

Supplementary material associated with this article can be found, in the online version, at doi:10.1016/j.virusres.2024.199518.

Data availability

Data will be made available on request.

References

Ades, AE, Soriano-Arandes, A, Alarcon, A, Bonfante, F, Thorne, C, Peckham, CS, et al., 2021. Vertical transmission of Zika virus and its outcomes: a Bayesian synthesis of prospective studies. Lancet Infect. Dis. 21 (4), 537–545.

Agrelli, A, De Moura, RR, Crovella, S, Brandão, LAC., 2019. ZIKA virus entry mechanisms in human cells. Infect. Genetic. Evolution 69, 22–29. April.

Arora, N, Sadovsky, Y, Dermody, TS, Coyne, CB, 2016. Microbial vertical transmission during human pregnancy, 20 (4), 412–426.

Assis, FL, Sippert, E, Rocha, BC, Volkova, E, Fares-Gusmao, R, Ok, S, et al., 2020. Genomic and phylogenetic analysis of Zika virus isolates from asymptomatic blood donors in the United States and Puerto Rico, 2016. Am. J. Trop. Med. Hyg. 102 (4), 880–883, 1 April.

Atieh, T, Nougairède, A, Klitting, R, Aubry, F, Failloux, AB, De Lamballerie, X, et al., 2017. New reverse genetics and transfection methods to rescue arboviruses in mosquito cells. Sci. Rep. 7 (1), 13983, 25 October.

Bayer, A, Lennemann, NJ, Ouyang, Y, Bramley, JC, Morosky, S, Torres, E, et al., 2017b. Type III Interferons produced by human placental Trophoblasts confer protection against Zika virus infection. Cell Host. Microbe 19 (5), 705–712.

Bayer, A, Lennemann, NJ, Ouyang, Y, Bramley, JC, Morosky, S, Torres, E, et al., 2017a. Type III interferons produced by human placental trophoblasts confer protection against Zika virus infection. Cell Host. Microbe 19 (5), 705–712.

Bolger, AM, Lohse, M, Usadel, B., 2014. Trimmomatic: a flexible trimmer for Illumina sequence data. Bioinformatics. 30 (15), 2114–2120, 1 August.

Brasil, P, Vasconcelos, Z, Kerin, T, Gabaglia, CR, Ribeiro, IP, Bonaldo, MC, et al., 2020. Zika virus vertical transmission in children with confirmed antenatal exposure. Nat. Commun. Dec. 11 (1), 3510.

Buranda, T, Wu, Y, Perez, D, Chigaev, A, Sklar, LA., 2010. Real-time partitioning of Octadecyl Rhodamine B into bead-supported lipid bilayer membranes revealing quantitative differences in Saturable binding sites in DOPC and 1:1:1 DOPC/SM/Cholesterol membranes. J. Phys. Chem. B. 114 (3), 1336–1349, 28 January.

Carbaugh, DL, Baric, RS, Lazear, HM., 2019. Envelope protein glycosylation mediates Zika virus pathogenesis. J. Virol. 93 (12), 1–16.

Carrera, J, Trenerry, AM, Simmons, CP, Mackenzie, JM., 2021. Flavivirus replication kinetics in early-term placental cell lines with different differentiation pathways. Virol J. Dec. 18 (1), 251.

Carro, AC, Damonte, EB., 2013. Requirement of cholesterol in the viral envelope for dengue virus infection. Virus. Res. 174 (1–2), 78–87.

Chen, Q, Gouilly, J, Ferrat, YJ, Espino, A, Glaziou, Q, Cartron, G, et al., 2020. Metabolic reprogramming by Zika virus provokes inflammation in human placenta. Nature Commun. [Internet] 11 (1). https://doi.org/10.1038/s41467-020-16754-z. Available on:

Ciota, AT, Kramer, LD., 2010. Insights into Arbovirus evolution and adaptation from experimental studies. Viruses. 2 (12), 2594–2617, 2 December.

Coyne, CB, Lazear, HM., 2016b. Zika virus — reigniting the TORCH. Nat. Rev. Microbiol. 14 (11), 707–715. November.

Coyne, CB, Lazear, HM., 2016a. Zika virus — reigniting the TORCH. Nat. Rev. Microbiol. 14 (11), 707–715. November.

Depristo, MA, Banks, E, Poplin, R, Garimella, KV, Maguire, JR, Hartl, C, et al., 2011. A framework for variation discovery and genotyping using next-generation DNA sequencing data. Nat. Genet.

Derek j. Platt. Zika virus-related neurotropic flaviviruses infect human placental explants and cause fetal demise in mice. 2018;44(426):61–70.

Einspieler, C, Utsch, F, Brasil, P, Panvequio Aizawa, CY, Peyton, C, Hydee Hasue, R, et al., 2019. Association of infants exposed to prenatal Zika virus infection with their clinical, neurologic, and developmental status evaluated via the general movement assessment tool. JAMa Netw. Open. 2 (1), e187235, 18 January.

Glycosylation of Zika virus is important in Host-Virus interaction and pathogenesis. 2019;(402).

Goellner, S, Enkavi, G, Prasad, V, Denolly, S, Eu, S, Mizzon, G, et al., 2023. Zika virus prM protein contains cholesterol binding motifs required for virus entry and assembly. Nat. Commun. 14 (1), 7344, 13 November.

Gollins, SW, Porterfield, JS., 1986. PH-dependent Fusion between the Flavivirus West Nile and liposomal model membranes. J. General Virol. 67 (1), 157–166, 1 January.

Guo, H, Rabouw, H, Slomp, A, Dai, M, Van Der Vegt, F, Van Lent, JWM, et al., 2018. Kinetic analysis of the influenza A virus HA/NA balance reveals contribution of NA to virus-receptor binding and NA-dependent rolling on receptor-containing surfaces. Lowen AC, curatore. PLoS Pathog. 14 (8), e1007233, 13 August.

Hafer, A, Whittlesey, R, Brown, DT, Hernandez, R., 2009. Differential incorporation of cholesterol by Sindbis virus grown in mammalian or insect cells. J. Virol. 83 (18), 9113–9121.

Hermanns, K, Göhner, C, Kopp, A, Schmidt, A, Merz, WM, Markert, UR, et al., 2018. Zika virus infection in human placental tissue explants is enhanced in the presence of dengue virus antibodies in-vitro. Emerg. Microbes. Infect. 7 (1), 198.

Hitakarun, A, Williamson, MK, Yimpring, N, Sornjai, W, Wikan, N, Arthur, CJ, et al., 2022. Cell type variability in the incorporation of lipids in the dengue virus Virion. Viruses. 14 (11), 2566, 19 November.

Joardar, A, Pattnaik, GP, Chakraborty, H., 2022. Mechanism of membrane fusion: interplay of lipid and peptide. J. Membrane Biol. 255 (2–3), 211–224. June.

Knöfler, M, Pollheimer, J., 2013. Human placental trophoblast invasion and differentiation: a particular focus on Wnt signaling. Front. Genet [Internet] 4 [citato 29 July 2024]Available on: http://journal.frontiersin.org/article/10.3389/fgene.2013.00190/abstract.

Lanciotti, RS, Kosoy, OL, Laven, JJ, Velez, JO, Lambert, AJ, Johnson, AJ, et al., 2008. Genetic and serologic properties of Zika virus associated with an epidemic, yap state, Micronesia, 2007. Emerg Infect Dis. 14 (8), 1232–1239. August.

Leier, HC, Messer, WB, Tafesse, FG., 2018. Lipids and pathogenic flaviviruses: an intimate union. PLoS. Pathog. 14 (5), 1–7.

Leier, HC, Weinstein, JB, Kyle, JE, Lee, JY, Bramer, LM, Stratton, KG, et al., 2020. A global lipid map defines a network essential for Zika virus replication. Nat. Commun. 11 (1), 1–15.

Li, H, Durbin, R., 2010. Fast and accurate long-read alignment with Burrows–Wheeler transform. Bioinformatics. 26 (5), 589–595, 1 March.

Li, H, Handsaker, B, Wysoker, A, Fennell, T, Ruan, J, Homer, N, et al., 2009. The Sequence Alignment/Map format and SAMtools. Bioinformatics. 25 (16), 2078–2079, 15 August.

Martin-Acebes, MA, Merino-Ramos, T, Blazquez, AB, Casas, J, Escribano-Romero, E, Sobrino, F, et al., 2014. The composition of west Nile virus lipid envelope unveils a role of Sphingolipid metabolism in Flavivirus biogenesis. J. Virol. 88 (20), 12041–12054.

Martín-Acebes, MA, Vázquez-Calvo, Á, Saiz, JC., 2016. Lipids and flaviviruses, present and future perspectives for the control of dengue, Zika, and West Nile viruses. Prog. Lipid Res. 64, 123–137.

Matrosovich M, Matrosovich T, Garten W, Klenk D. New low-viscosity overlay medium for viral plaque assays. 2006;7:1–7.

McKenna, A, Hanna, M, Banks, E, Sivachenko, A, Cibulskis, K, Kernytsky, A, et al., 2010. The genome analysis toolkit: a MapReduce framework for analyzing next-generation DNA sequencing data. Genome Res.

Melo, CFOR, De Oliveira, DN, De Oliveira Lima, E, Guerreiro, TM, Esteves, CZ, Beck, RM, et al., 2016. A lipidomics approach in the characterization of zika-infected mosquito cells: Potential targets for breaking the transmission cycle. PLoS. One 11 (10), 1–15.

Moncla, LH, Zhong, G, Nelson, CW, Dinis, JM, Mutschler, J, Hughes, AL, et al., 2016. Selective bottlenecks shape evolutionary pathways taken during mammalian adaptation of a 1918-like avian influenza virus. Cell Host. Microbe 19 (2), 169–180. February.

Müller, JA, Harms, M, Schubert, A, Jansen, S, Michel, D, Mertens, T, et al., 2016. Inactivation and environmental stability of Zika virus. Emerg. Infect. Dis. 22 (9), 1685–1687. September.

Nielsen-Saines, K, Brasil, P, Kerin, T, Vasconcelos, Z, Gabaglia, CR, Damasceno, L, et al., 2019. Delayed childhood neurodevelopment and neurosensory alterations in the second year of life in a prospective cohort of ZIKV-exposed children. Nat Med. 25 (8), 1213–1217. August.

Noronha, L de, Zanluca, C, Burger, M, Suzukawa, AA, Azevedo, M, Rebutini, PZ, et al., 2018. Zika virus infection at different pregnancy stages: anatomopathological findings, target cells and viral persistence in placental tissues. Front. Microbiol. 9 (September), 1–11.

Nour, AM, Li, Y, Wolenski, J, Modis, Y., 2013. Viral membrane fusion and Nucleocapsid delivery into the cytoplasm are distinct events in some Flaviviruses. Pierson TC, curatore. PLoS. Pathog. 9 (9), e1003585, 5 September.

Osuna-Ramos, JF, Reyes-Ruiz, JM, del Ángel, RM., 2018. The role of host cholesterol during Flavivirus infection. Front. Cell Infect. Microbiol. 8 (November), 1–12.

Perera, R, Riley, C, Isaac, G, Hopf-Jannasch, AS, Moore, RJ, Weitz, KW, et al., 2012. Dengue virus infection perturbs lipid homeostasis in infected mosquito cells. PLoS. Pathog. 8 (3).

Queiroz, A, Pinto, IFD, Lima, M, Giovanetti, M, de Jesus, JG, Xavier, J, et al., 2019. Lipidomic analysis reveals serum alteration of Plasmalogens in patients infected with ZIKA virus. Front. Microbiol. 10 (April), 1–10.
Rashid-Doubell, F, Tannetta, D, Redman, CWG, Sargent, IL, Boyd, CAR, Linton, EA., 2007. Caveolin-1 and lipid rafts in confluent BeWo Trophoblasts: evidence for Rock-1 association with Caveolin-1. Placenta. 28 (2–3), 139–151. February.
Reddy, T, Sansom, MSP., 2016. The role of the membrane in the structure and biophysical robustness of the dengue Virion envelope. Structure. 24 (3), 375–382. March.
Reed, LJ, Muench, H., 1938. A simple method of estimating fifty per cent endpoints. Am. J. Epidemiol.
Riemersma, KK, Jaeger, AS, Crooks, CM, Braun, KM, Weger-Lucarelli, J, Ebel, GD, et al., 2021. Rapid evolution of enhanced Zika virus virulence during direct vertebrate transmission chains. Parrish CR, curatore. J. Virol. 95 (8), 25 Marche02218-20.
Ripa, I, Andreu, S, López-Guerrero, JA, Bello-Morales, R., 2021. Membrane rafts: portals for viral entry. Front. Microbiol. 12, 631274, 4 February.
Robinson, KA, Akinyede, O, Dutta, T, Sawin, VI, Li, T, Spencer, MR, et al., 2013. Framework for Determining Research Gaps During Systematic Review: Evaluation [Internet]. Agency for Healthcare Research and Quality (US), Rockville (MD) [3 September 2022]. (AHRQ Methods for Effective Health Care). Available on: http://www.ncbi.nlm.nih.gov/books/NBK126708/.
Tabata, T, Petitt, M, Puerta-Guardo, H, Michlmayr, D, Wang, C, Fang-Hoover, J, et al., 2016. Zika virus targets different primary human placental cells, suggesting two routes for vertical transmission. Cell Host Microbe 20 (2), 155–166.
Thorvaldsdottir, H, Robinson, JT, Mesirov, JP., 2013. Integrative genomics viewer (IGV): high-performance genomics data visualization and exploration. Brief. Bioinform. 14 (2), 178–192, 1 March.
Van der Auwera, GA, Carneiro, MO, Hartl, C, Poplin, R, del Angel, G, Levy-Moonshine, A, et al., 2013. From fastQ data to high-confidence variant calls: the genome analysis toolkit best practices pipeline. Curr. Protoc. Bioinform.
van der Schaar, HM, Rust, MJ, Chen, C, van der Ende-Metselaar, H, Wilschut, J, Zhuang, X, et al., 2008. Dissecting the cell entry pathway of dengue virus by single-particle tracking in living cells. Farzan M, curatore. PLoS. Pathog. 4 (12), e1000244, 19 December.
Vial, T, Marti, G, Missé, D, Pompon, J., 2021. Lipid interactions between Flaviviruses and mosquito vectors. Front. Physiol. 12, 763195, 5 November.
Villalobos-Sánchez, E, Burciaga-Flores, M, Zapata-Cuellar, L, Camacho-Villegas, TA, DE, Elizondo-Quiroga, 2022. Possible routes for Zika virus vertical transmission in human placenta: a comprehensive review. Viral. Immunol. 35 (6), 392–403, 1 July.
Wilker, PR, Dinis, JM, Starrett, G, Imai, M, Hatta, M, Nelson, CW, et al., 2013. Selection on haemagglutinin imposes a bottleneck during mammalian transmission of reassortant H5N1 influenza viruses. Nat. Commun. 4 (1), 2636, 23 October.
Wilm, A, Aw, PPK, Bertrand, D, Yeo, GHT, Ong, SH, Wong, CH, et al., 2012. LoFreq: a sequence-quality aware, ultra-sensitive variant caller for uncovering cell-population heterogeneity from high-throughput sequencing datasets. Nucleic. Acids. Res. 40 (22), 11189–11201, 1 December.
Zaitseva, E, Yang, ST, Melikov, K, Pourmal, S, Chernomordik, LV., 2010. Dengue virus ensures its fusion in late endosomes using compartment-specific lipids. Diamond MS, curatore. PLoS. Pathog. 6 (10), e1001131, 7 October.